

Aspect-Ratio Scaling of the Domain-Wall Energy for the 2D $\pm J$ Random-Bond Ising Model

Ronald Fisch*

382 Willowbrook Dr., North Brunswick, NJ 08902

Alexander K. Hartmann†

Institut für Theoretische Physik, Universität Göttingen,
Friedrich-Hund Platz 1, 37077 Göttingen, Germany

(Dated: December 2, 2024)

The statistics of the domain-wall energy E_{dw} for ground states of the 2D random-bond Ising model with fractions p of -1 bonds and $(1-p)$ of $+1$ bonds are studied for $L \times M$ square lattices, as a function of the aspect ratio $R = L/M$. For $p = 0.5$, we study the limit $R \rightarrow 0$. We find that in this limit the results approximate the aspect-ratio scaling formulas of Carter, Bray and Moore, with stiffness exponent $\theta = 0$, unlike the previous results for large values of R . Furthermore, the probability distribution of E_{dw} approaches a Gaussian shape. We study also other values of p which are in the spin-glass region of the phase diagram. In particular we examine the way in which $\langle E_{dw} \rangle$ decays at fixed R as L increases. We find that the finite-size corrections can be described by the exponent $\omega \approx 2/3$, for all combinations (p, R) of parameter values we have studied.

I. INTRODUCTION

The spin glass phase^{1,2} is not stable at finite temperature in two dimensions (2D). When the energies are not quantized, the behavior at $T = 0$ can be understood in terms of a scaling theory,^{3,4} which is usually called the droplet model. This theory describes the scaling of the domain wall energy E_{dw} with length scale in terms of the stiffness exponent θ , which has a value of about -0.28 for 2D, almost independent of the detailed nature of the bond distribution.⁵ The possibility that quantization of the energies might lead to special behavior was first pointed out by Bray and Moore.⁶ It has become clear over the last few years that there actually is a fundamental difference in the behavior of the 2D Ising spin glass at zero temperature, between those cases where the energies are quantized and those where it is not.^{5,7,8}

The Hamiltonian of the Edwards-Anderson model for Ising spins is

$$H = - \sum_{\langle ij \rangle} J_{ij} S_i S_j, \quad (1)$$

where each spin S_i is a dynamical variable which has two allowed states, $+1$ and -1 . The $\langle ij \rangle$ indicates a sum over nearest neighbors on a simple square lattice of size $L \times M$. The standard model for quantized energies is the $\pm J$ model, where we choose each bond J_{ij} to be an independent identically distributed (iid) quenched random variable, with the probability distribution

$$P(J_{ij}) = p\delta(J_{ij} + 1) + (1-p)\delta(J_{ij} - 1). \quad (2)$$

Thus we actually set $J = 1$, as usual. The concentration of antiferromagnetic bonds is p , and $(1-p)$ is the concentration of ferromagnetic bonds. With the $P(J_{ij})$ of Eqn. (2), the EA Hamiltonian is equivalent to the Z_2 gauge glass model.⁹ Wang, Harrington and Preskill⁸ have

argued that the anomalous behavior of the $\pm J$ model is caused by topological long-range order, as a consequence of the gauge symmetry.

The first hint of the remarkable behavior of the $\pm J$ model was found by Wang and Swendsen.¹⁰ They found that, although for periodic boundary conditions there is an energy gap of $4J$ between the ground states and the first excited states, the specific heat when $T/J \ll 1$ appeared to be proportional to $\exp(-J/2T)$.

This result was questioned by Saul and Kardar.^{11,12} The behavior of the specific heat was finally demonstrated in a convincing fashion by Lukic *et al.*¹³ Saul and Kardar also found that the scaling of the domain-wall entropy with size did not appear to agree with the prediction of the droplet model.¹⁴ This issue has recently been clarified,¹⁵ and the entropy anomaly has been associated with zero-energy domain walls.

In this work we explore the behavior of E_{dw} for the $\pm J$ model under aspect-ratio scaling^{16,17}. For a square lattice of width L and height M , the aspect ratio is $R = L/M$. Carter, Bray and Moore¹⁸ have extended aspect-ratio scaling to the Ising spin glass, and demonstrated that studying the scaling as a function of R is an effective method for calculating the exponent θ . We will also study several cases where p is not equal to 0.5, so that the numbers of $+1$ and -1 bonds are unequal. We will find, in agreement with previous work on this model,^{5,7,19} that our results are consistent with $\theta = 0$. We will also find that the entire probability distribution $P(E_{dw})$ has a simple form for small R .

II. METHODS

We define domain walls for the spin glass as it was done in the seminal work of McMillan.²⁰ We look at differences in the ground-state energy between two samples with the same set of bonds, and the same boundary conditions in

one direction, but different boundary conditions in the other direction. For each set of bonds, the domain-wall energy, E_{dw} , is then defined to be the difference in the ground-state energies of the two different boundary conditions.

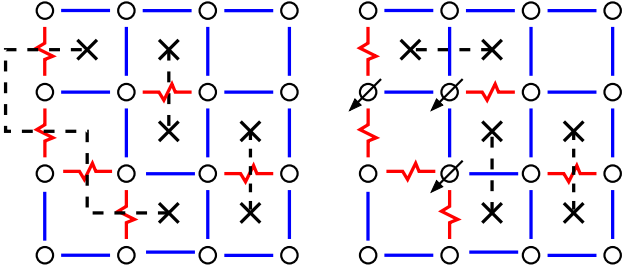


FIG. 1: (color online) 2D Ising spin glass with all spins up (left, up spins not shown). Straight lines are ferromagnetic, jagged lines are anti-ferromagnetic bonds. The dotted lines connect frustrated plaquettes (crosses). The bonds crossed by the dotted lines are unsatisfied. In the right part the ground state with three spins pointing down (all other up) is shown, corresponding to a minimum number of unsatisfied bonds.

We use a so called *matching algorithm* to calculate the ground states.^{21,22} Let us now explain just the basic idea of the matching algorithm. For the details, see Refs. 23,24,25. The algorithm allows us to find ground states for lattices which are planar graphs. This is the reason why we apply (anti-)periodic boundary conditions only in one direction, **x**, while the other direction, **y**, has free boundary conditions. In the left part of Fig. 1 a small 2D system with (for simplicity) free boundary conditions in both directions is shown. All spins are assumed to be “up”, hence all anti-ferromagnetic bonds are not satisfied. If one draws a dotted line perpendicular to each unsatisfied bond, one ends up with the situation shown in the figure: all dotted lines start or end at frustrated plaquettes and each frustrated plaquette is connected to exactly one other frustrated plaquette by a dotted line. Each pair of plaquettes is then said to be *matched*. Closed loops of broken bonds unrelated to frustrated plaquettes can also appear in general, but this is possible only for excited states. Now, one can consider the frustrated plaquettes as the vertices and all possible pairs of connections as the edges of a (dual) graph. The dotted lines are selected from the edges connecting the vertices and called a *perfect matching*, since *all* plaquettes are matched. One can assign weights to the edges in the dual graph, the weights are equal to the sum of the absolute values of the bonds crossed by the dotted lines. The weight Λ of the matching is defined as the sum of the weights of the edges contained in the matching. As we have seen, Λ counts the broken bonds, hence, the energy of the configuration is given by

$$E = - \sum_{\langle i,j \rangle} |J_{ij}| + 2\Lambda, \quad (3)$$

with $|J_{ij}| = 1$ from Eqn. (2). Note that this holds for

any configuration of the spins, if one includes also closed loops in Λ , since a corresponding matching always exists.

Obtaining a ground state means minimizing the total weight of the broken bonds (see right panel of Fig. 1). This automatically forbids closed loops of broken bonds, so one is looking for a *minimum-weight perfect matching*. This problem is solvable in polynomial time. The algorithms for minimum-weight perfect matchings^{26,27} are among the most complicated algorithms for polynomial problems. Fortunately the LEDA library offers a very efficient implementation,²⁸ which we have applied here.

With free boundary conditions in at least one direction, E_{dw} is a multiple of 2 (since $J = 1$). When periodic or antiperiodic boundary conditions are applied in both the **x** and **y** directions, however, E_{dw} becomes a multiple of 4 if the number of -1 bonds is even. If the number of -1 bonds is odd, E_{dw} takes on values $(4n + 2)$ with these boundary conditions. When M is odd, changing the boundary conditions in the **x** direction from periodic to antiperiodic changes the number of -1 bonds from odd to even, or vice versa.

The behavior of the domain-wall energy for the $\pm J$ model with $R > 1$ was discussed previously.²⁹ For the boundary conditions we are using, the average $\langle |E_{dw}| \rangle$ goes to zero exponentially as R becomes much greater than one. Here $\langle \dots \rangle$ denotes an average over the ensemble of random bond distributions for an $L \times M$ lattice. We can understand this result by thinking of the system as consisting of blocks of size $M \times M$ pasted together along the **x** direction. The probability of having a zero-energy domain wall in each block is almost independent of the other blocks. The same thing happens when M is even if the boundary conditions in the **y** direction are periodic or antiperiodic. However, if M is odd and the boundary conditions in the **y** direction are periodic or antiperiodic, $\langle |E_{dw}| \rangle$ goes to 2 at large R , because then $E_{dw} = 0$ is not allowed. Since a critical exponent should be independent of boundary conditions, this is a(nother) demonstration that $\theta = 0$ for the $\pm J$ model in 2D.

As pointed out earlier²⁹, these results for large R do not agree with the scaling law prediction of Carter, Bray and Moore,¹⁸ due to the special role of zero-energy domain walls. On the other hand, in the limit $R \rightarrow 0$ with our boundary conditions, the prediction of Carter, Bray and Moore is

$$\langle |E_{dw}| \rangle \sim L^\theta (M/L)^{(d-1)/2}, \quad M \gg L. \quad (4)$$

This limit has not been studied before for the $\pm J$ model. When $\theta = 0$, $\langle |E_{dw}| \rangle$ should scale as $R^{-1/2}$ in 2D. For small R we may think of the lattice as consisting of $L \times L$ subsystems stacked in the **y** direction, with E_{dw} being the sum of the domain-wall energies of the subsystems. Therefore, by the central limit theorem, we anticipate that the probability distribution of E_{dw} should approach a Gaussian distribution in the limit of small R . In the spin-glass region of the phase diagram, the center of this limiting Gaussian will approach zero as L increases. We will show that our numerical results for the small R limit

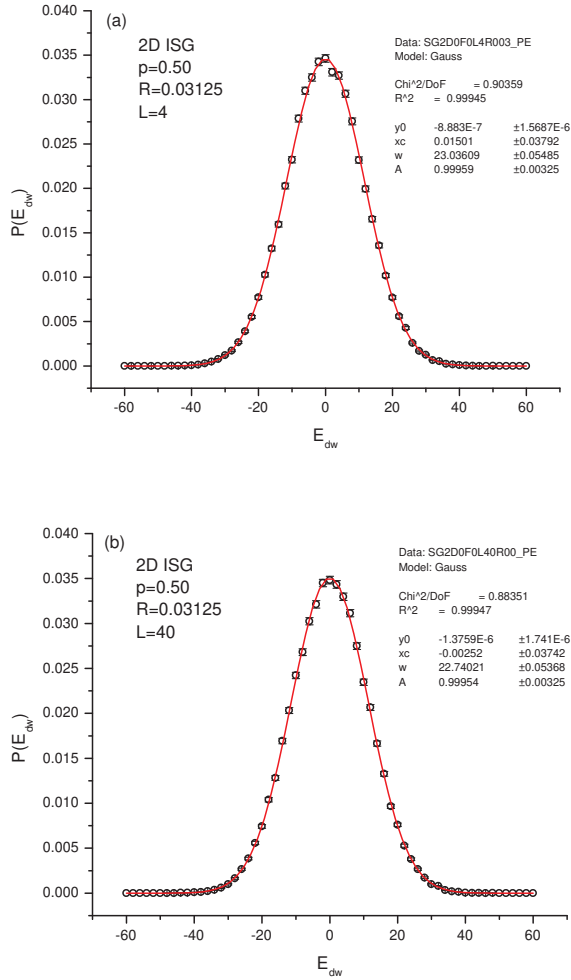


FIG. 2: (color online) Probability distributions of the domain-wall energy, $P(E_{dw})$, for $p = 0.5$ and $R = 1/32$: (a) $L = 4$, $M = 128$; (b) $L = 40$, $M = 1280$. The error bars show one standard deviation.

are indeed in good agreement with these expectations.

III. NUMERICAL RESULTS

When $p = 1/2$ the distribution $P(J_{ij})$ of Eqn. (2) is symmetric about zero. Thus in this case the distribution $P(E_{dw})$ is (ignoring statistical fluctuations) also symmetric around zero, for any values of L and M . Therefore, we used $p = 1/2$ to collect data for sets of random lattices with sequences of L and M having the aspect ratios $R = 1, 1/2, 1/4, 1/8, 1/16$ and $1/32$. For each value of R , we then used finite-size scaling to extrapolate to the large lattice limit.

In Fig. 2 we show the probability distributions $P(E_{dw})$ for sets of lattices with $p = 1/2$ and $R = 1/32$, for $L = 4$ and $L = 40$. In each case, there are 90,000 random sam-

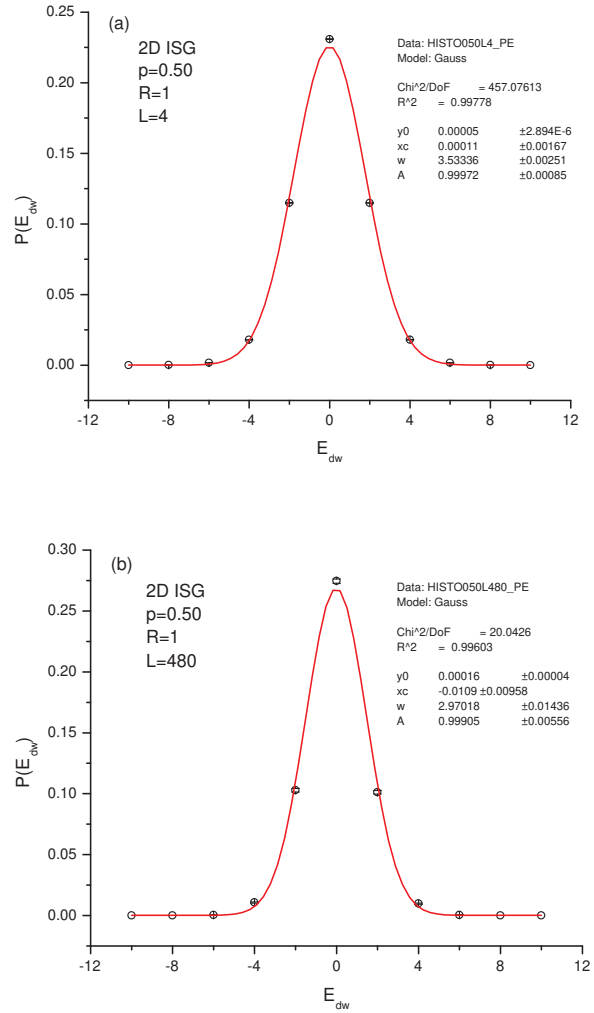


FIG. 3: (color online) Probability distributions of the domain-wall energy, $P(E_{dw})$, for $p = 0.5$ and $R = 1$: (a) $L = 4$, $M = 4$; (b) $L = 480$, $M = 480$. The error bars show one standard deviation.

ples in the data set. Each distribution was fit to a Gaussian using the Origin 6.0 Professional³⁰ fitting program. These fits are quite good, which verifies that the approximation of thinking of the $R = 1/32$ sample as 32 independent subsystems stacked along the y axis is a good one. The reader should also note that we find no evidence for any "sawtooth" structure in the data. This is in marked contrast to the case of periodic or antiperiodic boundary conditions in the y direction, which causes alternate values of E_{dw} to have zero probability. Therefore $P(E_{dw})$ does not become independent of the boundary conditions even in the limit of large lattices. This is an aspect of the topological long-range order⁸ which exists in this model when the boundary conditions are periodic along both x and y .

In Fig. 3 we show $P(E_{dw})$ for sets of lattices with $p =$

$1/2$ and $R = 1$, for $L = 4$ and $L = 480$. The number of samples is 940,000 for $L = 4$, and 20,054 for $L = 480$. These $R = 1$ data were taken from earlier work.¹⁹ The effects of energy quantization are more obvious for $R = 1$ than for smaller R , since the distributions are narrower. These distributions have more weight at $E_{dw} = 0$ than the best Gaussian fits. The L dependence of the width of each distribution is also larger than for $R = 1/32$.

Because the shape of the $P(E_{dw})$ distribution is changing with R , we expect that the aspect-ratio scaling will not be perfect in the range of our data. As we shall see, however, the deviations from the Gaussian fit become smaller than our statistical errors by $R = 1/4$. Thus we are able to verify that we are approaching the predicted scaling results. The reader should note that the fitting program³⁰ ignores the fact that the distribution is quantized.

IV. FINITE-SIZE SCALING ANALYSIS

The next step in the analysis is to extrapolate our finite-size lattice data to the large L limit. We do this by fitting the data to a form

$$F(R, L) = A(R) + \sum_{m=1}^{m^*} B_m L^{-m\omega}, \quad (5)$$

with $\omega = 2/3$. $F(R, L)$ represents any function of $P(E_{dw})$. Two examples of these that we chose to look at were $\langle |E_{dw}| \rangle$ and the probability $P(E_{dw} = 0)$.

The number of correction-to-scaling terms included, m^* , was chosen according to the amount of data to be fitted, and was usually 2 or 3. Of course, the values of the coefficients A and B_m which are found by the fitting program³⁰ depend somewhat on the choice of m^* . The statistical errors computed by the fitting program do not include any allowance for systematic errors due to the choice of the form of the scaling function. Fortunately, the value of A is relatively insensitive to the choice of m^* .

It turned out, in general, that whether we chose m^* to be 2 or 3, the B_m coefficients did not all have the same sign. This effect is caused by the behavior at small L . For this reason, there is no well defined prescription for deciding what the best choice of the exponent ω is. The value $\omega = 2/3$ was chosen empirically, and is similar to the values used previously in other work on this model.^{7,8} For a critical point with $T_c > 0$, the general theory of finite-size scaling³¹ requires that $\omega = 1/\nu$, where ν is the correlation length exponent. That result does not apply here, however, since $T_c = 0$.

Our finite-size scaling fits to the data using Eqn. (5) for the case $p = 0.5$ and $R = 1$ are shown in Fig. 4. In the figures, we show $F(R, L)$ as a function of $L^{-2/3}$. The same $R = 1$ data was originally¹⁹ fit by making different assumptions which are not consistent with Eqn. (5).

When $p = 0.5$ the configuration averages of all the odd moments of $P(E_{dw})$ must vanish. Therefore the domi-

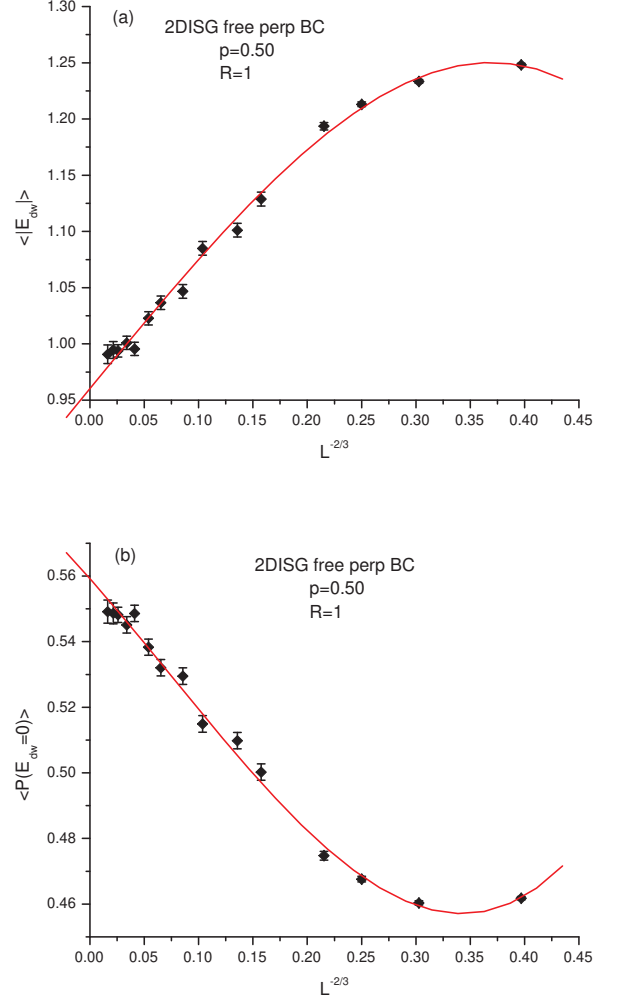


FIG. 4: (color online) Finite-size scaling fits for $p = 0.5$ and $R = 1$: (a) $\langle |E_{dw}| \rangle$ vs. $L^{-2/3}$; (b) probability of $E_{dw} = 0$ vs. $L^{-2/3}$. The error bars show one standard deviation.

nant contribution to non-Gaussian behavior will be the kurtosis, $m_4/(m_2)^2 - 3$, where m_i is the i^{th} moment of $P(E_{dw})$. Fig. 5 shows the behavior of the kurtosis of the $P(E_{dw})$ distributions at $p = 0.5$ as a function of L and R . It shows that for $R \leq 1/4$ the kurtosis is negligible except when $L < 8$, quantifying the convergence towards a Gaussian distribution for small aspect ratios.

In Table I we show the results of the finite-size scaling fits for $\langle |E_{dw}| \rangle$ at $p = 0.5$. According to Eqn. (4), the prediction of aspect-ratio scaling theory is that the ratio $A(R)/A(2R)$ should approach $\sqrt{2} \approx 1.414$ for small R . Considering the statistical errors and the corrections to scaling, the agreement is quite satisfactory.

Table II shows the results of the finite-size scaling fits for the probability that $E_{dw} = 0$ at $p = 0.5$. Since, from the central limit theorem, for the sum Σ of K suitably iid integers, $P(\Sigma = 0) \sim K^{-0.5}$, via $K \sim R^{-1}$ the prediction

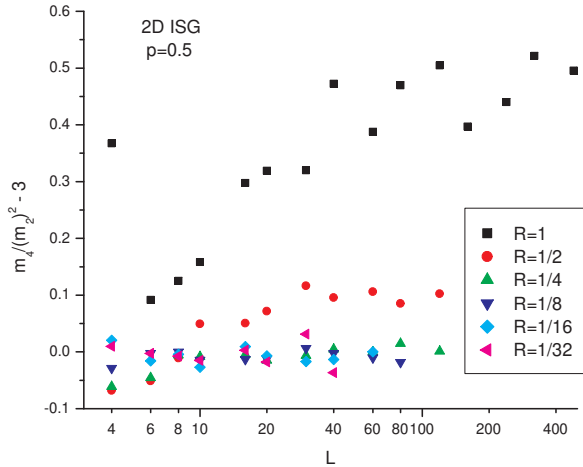


FIG. 5: (color online) Kurtosis vs. R for $p = 0.5$. The x axis is scaled logarithmically.

TABLE I: $\langle |E_{dw}| \rangle$ for $p = 0.5$, extrapolated to $L = \infty$, as a function of the aspect ratio, R . The m^* and A are defined by Eqn. (5), and the eA are statistical error estimates.

R	m^*	A	eA	$A(R)/A(2R)$
1.0	3	0.96025	0.00792	
0.5	2	1.81967	0.00471	1.895
0.25	2	2.89085	0.00671	1.589
0.125	2	4.28859	0.01013	1.484
0.0625	2	6.21247	0.02387	1.449
0.03125	1	8.98954	0.03402	1.447

of aspect-ratio scaling theory for this quantity is that the ratio $A(R)/A(2R)$ should approach $1/\sqrt{2} \approx 0.707$ for small R . Again, the agreement is about as good as could be expected.

V. FINITE-SIZE SCALING FOR $p \neq 1/2$

When $p \neq 0.5$, $P(J_{ij})$ from Eqn. (2) is not symmetric about zero. Therefore, for a finite lattice, $P(E_{dw})$ will not

TABLE II: Probability of $E_{dw} = 0$ for $p = 0.5$, extrapolated to $L = \infty$, as a function of the aspect ratio, R . The m^* and A are defined by Eqn. (5), and the eA are statistical error estimates.

R	m^*	A	eA	$A(R)/A(2R)$
1.0	3	0.55921	0.00294	
0.5	3	0.33215	0.00261	0.594
0.25	2	0.21619	0.00135	0.651
0.125	2	0.14736	0.00139	0.682
0.0625	2	0.10264	0.00144	0.697
0.03125	1	0.07053	0.00069	0.687

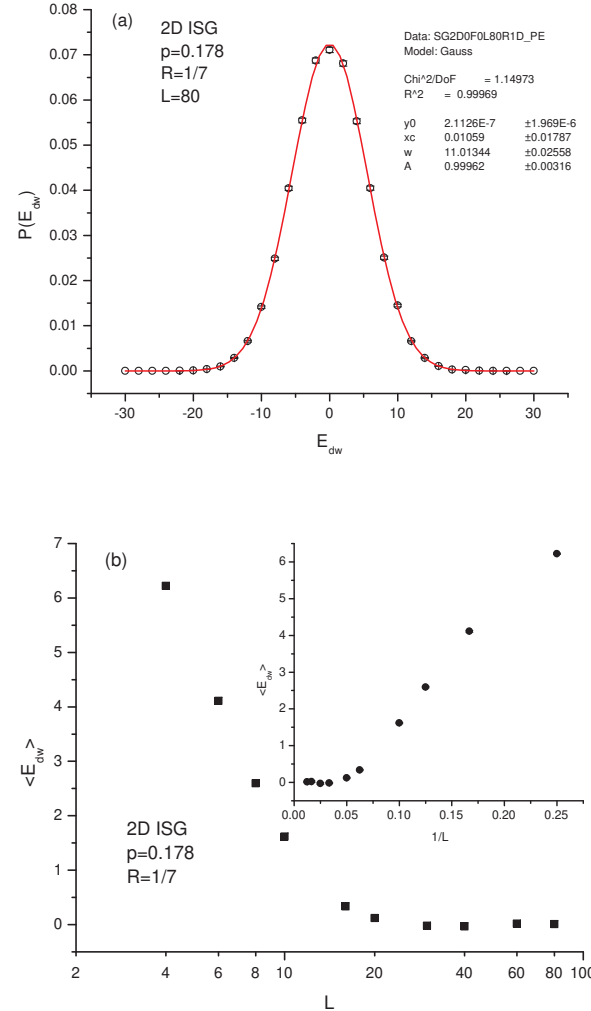


FIG. 6: (color online) Data for $p = 0.178$ and $R = 1/7$: (a) Probability distribution of the domain-wall energy, $P(E_{dw})$, for $L = 80$, $M = 560$. The error bars show one standard deviation. (b) $\langle E_{dw} \rangle$ vs. L . The x axis is scaled logarithmically, and the error bars are smaller than the plotting symbols. The inset shows $\langle E_{dw} \rangle$ vs. $1/L$.

be symmetric about zero either, *i.e.* the odd moments of $P(E_{dw})$ will no longer have a configuration average of zero. In the spin-glass region of the phase diagram, however, the asymmetric part of $P(E_{dw})$ is expected to vanish as the size of the lattice become large compared to the ferromagnetic correlation length. To demonstrate how this works for $R < 1$, we show computed results for the probability distributions $P(E_{dw})$ for $p = 0.178$ and $R = 1/7$ in Fig. 5, and for $p = 0.15$ and $R = 1$ in Fig. 6. We have also done calculations for several other values of p between 0.15 and 0.5 at $R = 1$.

Fig. 6(a) shows that for $R = 1/7$ the distribution is close to a Gaussian centered at zero for large L . In Fig. 6(b) we show the decay of the average of E_{dw} as L in-

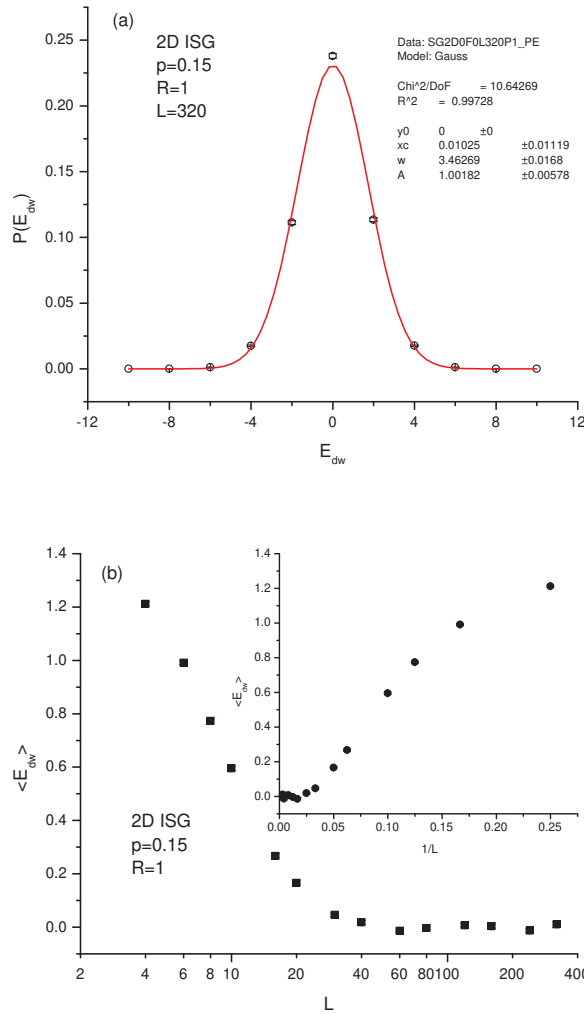


FIG. 7: (color online) Data for $p = 0.15$ and $R = 1$: (a) Probability distribution of the domain-wall energy, $P(E_{dw})$, for $L = 320$, $M = 320$. The error bars show one standard deviation. (b) $\langle E_{dw} \rangle$ vs. L . The x axis is scaled logarithmically, and the error bars are smaller than the plotting symbols. The inset shows $\langle E_{dw} \rangle$ vs. $1/L$.

creases. The decay is approximately $1/L$ for small L (see inset). For larger L , however, the first moment of the distribution goes to zero much more rapidly than $1/L$. (We obtained $\sim L^{-3.5}$ from a fit).

In Fig. 7(a) we see that for $p = 0.15$ and $R = 1$ the behavior at large L becomes essentially the same as what we found in the $p = 0.5$ case, in Fig. 3. Fig. 7(b) shows that, when p gets close to the ferromagnet-spin glass multicritical point, the decay of the $\langle E_{dw} \rangle$ distribution at small L is very slow. The behavior at larger L is qualitatively the same as found in Fig. 6(b). For values of p even closer to the multicritical point,³² we would see $\langle E_{dw} \rangle$ rise at small L , reach a maximum at the ferromagnetic correlation length, (which diverges as the multicritical point is

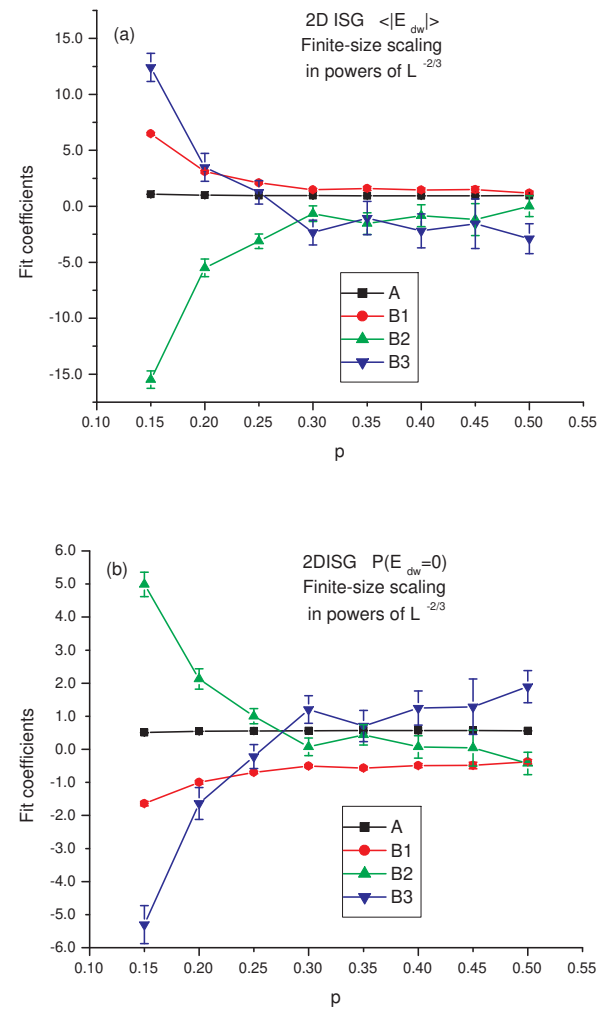


FIG. 8: (color online) Fit coefficients (defined by Eqn. (5)) for $R = 1$: (a) $\langle |E_{dw}| \rangle$ vs. p ; (b) $P(E_{dw} = 0)$ vs. p .

approached), and then fall to zero as L becomes large.

Fig. 8(a) shows the fit coefficients for $\langle |E_{dw}| \rangle$, as defined by Eqn. (5), as a function of p for $R = 1$. We see that the value of A , the estimate for $L \rightarrow \infty$, changes very little over this range of p , even though there are substantial variations in the B_m coefficients. Note that the B_m alternate in sign for the smaller values of p . If one tried to fit the finite-size scaling with a single power-law term instead of using the series of Eqn. (5), this would give rise to an apparent exponent ω_{eff} which was decreasing as p approached the multicritical point. In Fig. 8(b) the results of fitting $P(E_{dw} = 0)$, which shows the same type of behavior, are given.

VI. SUMMARY

We have studied the statistics of domain-wall energies for ground states of the 2D Ising spin glass with an equal mixture of $+1$ and -1 bonds for $L \times M$ square lattices with aspect ratio R between $1/32$ and 1 . We have also studied several values of p between 0.15 and 0.5 , where p is the fraction of negative bonds. We find that for large lattices the probability distribution of E_{dw} in the spin-glass region of the phase diagram approaches a Gaussian centered at $E = 0$. In the small R limit the behavior obeys the aspect-ratio scaling predictions of Carter, Bray and Moore with the stiffness exponent $\theta = 0$. For $0.15 \leq p < 0.5$, the value of $\langle E_{dw} \rangle$ decays to zero slowly at small L , and then very rapidly at larger L . The finite-size corrections of $\langle |E_{dw}| \rangle$ and of the probability that $E_{dw} =$

0 can be described by a correction-to-scaling exponent $\omega = 2/3$ for all values of p in the spin-glass region. Higher order corrections become larger as the multicritical point is approached.

Acknowledgments

RF is grateful to S. L. Sondhi, F. D. M. Haldane and D. A. Huse for helpful discussions, and to Princeton University for providing use of facilities. AKH acknowledges financial support from the *VolkswagenStiftung* (Germany) within the program “Nachwuchsgruppen an Universitäten” and from the DYGLAGEMEN program funded by the EU.

^{*} ron@princeton.edu
[†] hartmann@physik.uni-goettingen.de

¹ S. F. Edwards and P. W. Anderson, *J. Phys. F* **5**, 965 (1975).
² Reviews on spin glasses can be found in: K. Binder and A. P. Young, *Rev. Mod. Phys.* **58**, 801 (1986); M. Mezard, G. Parisi, M. A. Virasoro, *Spin Glass Theory and Beyond*, (World Scientific, Singapore 1987); K. H. Fischer and J. A. Hertz, *Spin Glasses*, (Cambridge University Press, Cambridge 1991); A. P. Young (ed.), *Spin Glasses and Random Fields*, (World Scientific, Singapore 1998).
³ A. J. Bray and M. A. Moore, *Phys. Rev. B* **31**, 631 (1985).
⁴ D. S. Fisher and D. A. Huse, *Phys. Rev. Lett.* **56**, 1601 (1986).
⁵ C. Amoruso, E. Marinari, O. C. Martin and A. Pagnani, *Phys. Rev. Lett.* **91**, 087201 (2003).
⁶ A. J. Bray and M. A. Moore, *Heidelberg Colloquium on Glassy Dynamics*, J. L. van Hemmen and I. Morgenstern, (ed.), (Springer, Berlin, 1986), pp. 121-153.
⁷ A. K. Hartmann and A. P. Young, *Phys. Rev. B* **64**, 180404(R) (2001).
⁸ C. Wang, J. Harrington and J. Preskill, *Ann. Phys. (N.Y.)* **303**, 31 (2003).
⁹ Y. Ozeki and H. Nishimori, *J. Phys. A* **26**, 3399 (1993).
¹⁰ J.-S. Wang and R. H. Swendsen, *Phys. Rev. B* **38**, 4840 (1988).
¹¹ L. Saul and M. Kardar, *Phys. Rev. E* **48**, R3221 (1993).
¹² L. Saul and M. Kardar, *Nucl. Phys. B* **432**, 641 (1994).
¹³ J. Lukic, A. Galluccio, E. Marinari, O. C. Martin and G. Rinaldi, *Phys. Rev. Lett.* **92**, 117202 (2004).
¹⁴ D. S. Fisher and D. A. Huse, *Phys. Rev. B* **38**, 386 (1988).
¹⁵ R. Fisch, *cond-mat/0508468*.
¹⁶ A. E. Ferdinand and M. E. Fisher, *Phys. Rev.* **185**, 832 (1969).
¹⁷ H. Park and M. den Nijs, *Phys. Rev. B* **38**, 565 (1988).
¹⁸ A. C. Carter, A. J. Bray and M. A. Moore, *Phys. Rev. Lett.* **88**, 077201 (2002).
¹⁹ I. A. Campbell, A. K. Hartmann and H. G. Katzgraber, *Phys. Rev. B* **70**, 054429 (2004).
²⁰ W. L. McMillan, *Phys. Rev. B* **29**, 4026 (1984).
²¹ A. K. Hartmann and H. Rieger, *Optimization Algorithms in Physics*, (Wiley-VCH, Berlin, 2001).
²² A. K. Hartmann and H. Rieger, *New Optimization Algorithms in Physics*, (Wiley-VCH, Berlin, 2004).
²³ I. Bieche, R. Maynard, R. Rammal, and J. P. Uhry, *J. Phys. A* **13**, 2553 (1980).
²⁴ F. Barahona, R. Maynard, R. Rammal, and J. P. Uhry, *J. Phys. A* **15**, 673 (1982).
²⁵ U. Derigs and A. Metz, *Math. Prog.* **50**, 113 (1991).
²⁶ W. J. Cook, W. H. Cunningham, W. R. Pulleyblank, and A. Schrijver, *Combinatorial Optimization*, (John Wiley & Sons, New York 1998).
²⁷ B. Korte and J. Vygen, *Combinatorial Optimization - Theory and Algorithms*, (Springer, Heidelberg 2000).
²⁸ K. Mehlhorn and St. Näher, *The LEDA Platform of Combinatorial and Geometric Computing* (Cambridge University Press, Cambridge 1999); see also <http://www.algorithmic-solutions.de>.
²⁹ A. K. Hartmann, A. J. Bray, A. C. Carter, M. A. Moore and A. P. Young, *Phys. Rev. B* **66**, 224401 (2002).
³⁰ ©OriginLab Corporation, Northampton, MA 01060.
³¹ M. N. Barber, in *Phase Transitions and Critical Phenomena, Vol. 8*, C. Domb and J. L. Lebowitz (ed.), (Academic, London, 1983), pp. 145-266.
³² C. Amoruso and A. K. Hartmann, *Phys. Rev. B* **70**, 134425 (2004).